Materials and Design 97 (2016) 372–380

Contents lists available at ScienceDirect

Materials and Design

journal homepage: www.elsevier.com/locate/matdes

High-resolution high-speed nanoindentation mapping of cement pastes: Unravelling the effect of microstructure on the mechanical properties of hydrated phases

M. Sebastiani [a,*], R. Moscatelli [a], F. Ridi [b], P. Baglioni [b], F. Carassiti [a]

[a] Roma" TRE University, via della Vasca Navale 79, 00146 Rome (Italy)
[b] Department of Chemistry "Ugo Schiff" & CSGI, University of Florence, Florence, Italy

ARTICLE INFO

Article history:
Received 8 January 2016
Received in revised form 19 February 2016
Accepted 20 February 2016
Available online 26 February 2016

Keywords:
Cement
Nanoindentation
High-speed
Statistical
Mapping
Packing density

ABSTRACT

Cementitious materials represent the most used materials in the construction industry. Their strong heterogeneity and multiscale microstructure make the study of the mechanical properties and the in-service behaviour very challenging: new techniques are required by industrial research to better investigate these aspects. In this work a novel technique based on statistical nanoindentation is exploited to obtain results about the microstructure build-up and the mechanical properties. An innovative high-speed nanoindentation method is here combined and compared with a standard nanoindentation procedure in order to get highly consistent statistical results. Combining the high-speed nanoindentation, the statistical deconvolution and SEM/EDS investigations, the main phases present in the tested hydrated cement paste have been characterized. High-resolution maps of the mechanical properties are in good agreement with SEM-EDS results. The evolution of the mechanical properties has been tested over the time and in particular after 1, 3, 5, 7, 14 and 28 days of hydration. It was found that the nano-mechanical properties were almost constant during the hydration time and the evolution of the bulk mechanical resistance properties of the cement paste is found to be due to a variation of the volume proportions between the three principal phases (low-density, high-density and ultra-high-density C–S–H).

1. Introduction

Cement-based composites still represent the most used materials in the construction industry, due to their low production and processing costs. Nonetheless, the fundamental mechanisms underlying the microstructure build-up and the in-service mechanical behaviour are still mostly unknown, due to the extreme complexity of such materials [1].

Cement is a heterogeneous material, composed by multiple phases and whose final structure shows multi-scale features, ranging from nanometres (colloidal nanometric units) to tens of micrometres (large capillary pores). A large part of the literature has described the colloidal nature of the main hydrated phase in cement paste: calcium silicate hydrate (shortly C–S–H) has been the subject of intensive research, due to its relevance in determining the mechanical properties of the whole material. C–S–H is known to have a nanogranular nature, made of nanometric (~5 nm) building blocks [2,3] whose aggregation produces the interconnected network that binds together the entire matrix [4]. Such complexity is further increased due to the extensive use of additives [5,6]. Today, chemical admixtures are essential components of every formulation: many species of organic products are used to influence the hydration kinetics (retarders or accelerators), to confer fluidity without adding excess water (superplasticizers) or to control the plasticity of the paste (viscosity modifiers). In addition, inorganic additives are increasingly used: for example the so-called "supplementary cementitious materials" (SCM) are silica-based by-products from different industrial activities that display pozzolanic properties and are added with the final aim of obtaining a significant reduction in the CO_2 emissions per ton of cementitious materials [7]. Several other nanoparticles are finally introduced in cement formulation, to confer special properties [8]. All these additions inevitably affect the morphology of the hydrated phases, especially of C–S–H [9–12]. As a consequence of their influence on the structure, the admixtures may also have a significant influence on the mechanical properties of C–S–H and on the entire specimen. In particular, it is well known [13] that gaining the full control over the mechanical performance of a cement-based structure requires the relationship among the nanoscale mechanical properties, the structure and composition at the nanoscale to be clearly understood. For this reason, as the industrially used formulations of cement and concrete become increasingly complex, basic research efforts are required to provide industry with methods for nanoscale, or multi-scale, characterization of cement-based materials [14–16].

Despite several studies [13,17–18] have been reported on the investigation of the mechanical properties of the hydration products in Portland cement pastes, especially of C–S–H, the full assessment of the

* Corresponding author.
E-mail address: marco.sebastiani@uniroma3.it (M. Sebastiani).

http://dx.doi.org/10.1016/j.matdes.2016.02.087
0264-1275/

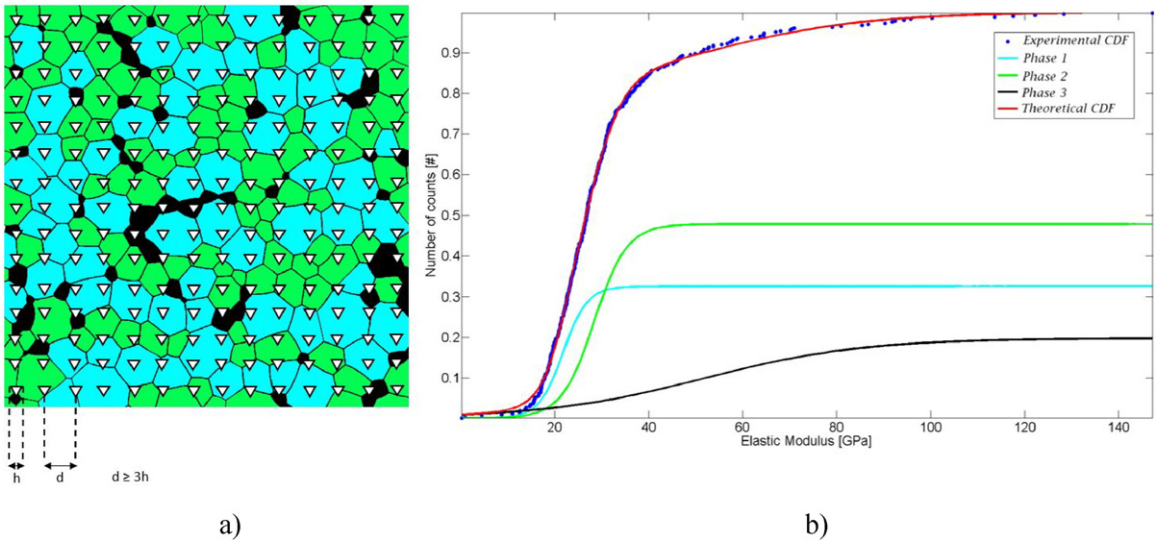

Fig. 1. Concept of statistical nanoindentation to map the mechanical properties of multi-phase materials. (a) a grid of tests is performed on a generic multi-phase material and (b) the cumulative distribution function plot of obtained properties (elastic modulus and/or hardness) are analyzed through deconvolution processes, in order to identify mechanical phases.

correlation between mechanical properties, composition and nanostructure is not completely assessed, so far.

Most of the literature agrees on the existence of at least two different C–S–H phases in Portland cement pastes, differing for the packing density of the nanometric elementary building blocks. According to the colloidal model firstly developed by Hamlin M. Jennings [3] these phases are named as high-density (HD) and low-density (LD) C–S–H: these products have similar composition and different intrinsic values of hardness and elastic modulus, these properties being independent on the mix proportions of the paste, which only contribute to the relative volume of HD and LD C–S–H.

The mechanical properties depend on two main factors:

a) the packing density of the nanometric units, which determines the nano- and micro-porosity. According to the literature, the packing density of LD C–S–H approaches $\eta \approx 0.64$, the typical value for the random close-packed (RCP) limit of spheres [19], while the HD C–S–H displays a packing density value of $\eta \approx 0.74$, typical of a hexagonal close-packed (hcp) arrangement [20]. Due to the different spatial arrangement of the basic units, the estimated porosity in HD C–S–H and LD C–S–H is 26% and 36%, respectively [18].
b) The Ca/Si ratio. It is well known that this ratio is directly correlated to the length of the silicate chains constituting the layers inside the nanometric units [21–23]. In particular the polymerization of the silicate chain increases with decreasing Ca/Si.

The way the Ca/Si (or the polymerization degree) affects the mechanical properties is not fully understood, due to the difficulty to decouple this effect from the influence of the porosity or the possible entanglement of C–S–H with other phases (such as $Ca(OH)_2$). For these reasons, the debate on this topic is still open, as some authors have claimed that HD C–S–H usually displays a Ca/Si ratio lower than LD C–S–H [24,25] while other groups [26,27] reached the opposite conclusion.

A third phase, Ultra-High-Density (UHD) C–S–H phase, in addition to the already known LD C–S–H and HD C–S–H phases, was recently proposed as well [28]. The mechanical properties of this UHD C–S–H phase follow similar packing density scaling relations as LD C–S–H and

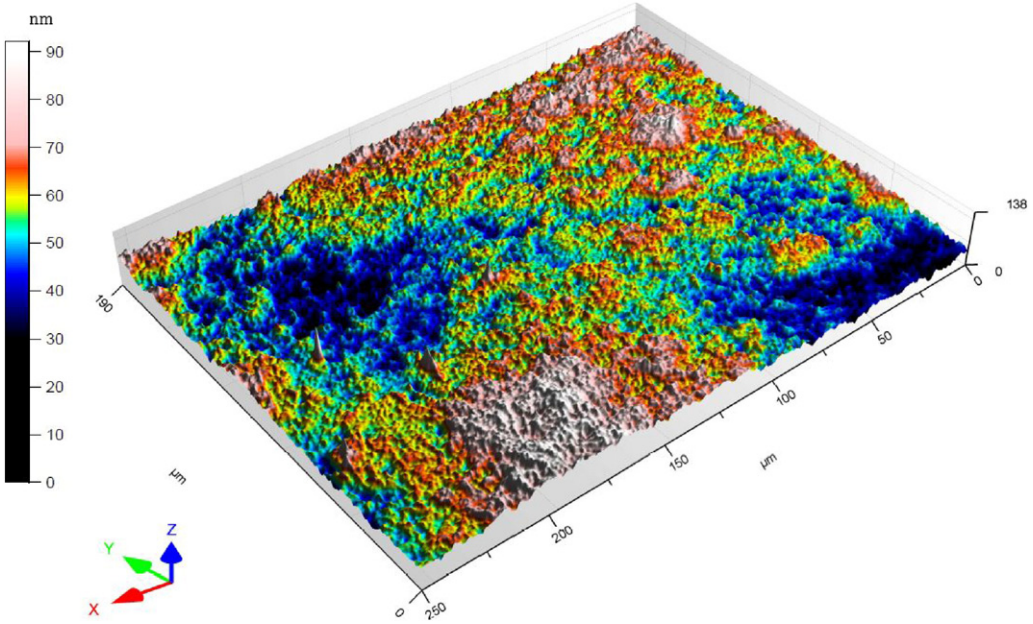

Fig. 2. Surface morphology of the paste cement sample after the complete polishing treatment.

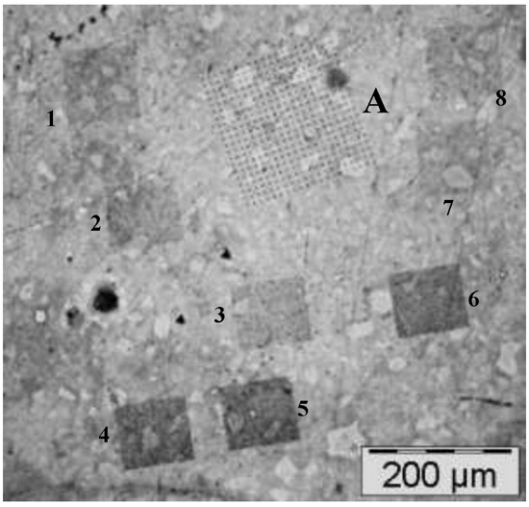

Fig. 3. Optical micrograph where eight different maps (squared areas in dark grey, labels 1–8) obtained by high-speed nanoindentation can be compared with the one obtained by conventional CSM nanoindentation (label "A").

HD C–S–H. This suggests that the UHD C–*S*–H phase is structurally distinct but compositionally similar to the other C–S–H phases. UHD C–S–H phase has a packing density of $\eta \approx 0.83$, which comes remarkably close to a two-scale limit random packing of $0.64 + (1–0.64) * 0.64 = 0.87$.

In recent years, statistical nanoindentation (or nanoindentation mapping) has been proposed as a valuable tool for the characterization of nanoscale mechanical properties of cement paste. The method, which was originally proposed in 2004 [13], consists in the achievement of a grid of nanoindentation experiments on a polished sample, followed by the statistical deconvolution of the elastic modulus results in order to identify the mechanical properties and distribution of the mechanical phases that are present in the material at the nano-scale. Several papers have shown the possibility of identifying the different C–S–H phases in cement pastes by means of this technique [29].

The principle of statistical nanoindentation is described in Fig. 1a–b. Assuming that the distribution of the elastic modulus (E) is well approximated by a Gaussian distribution, the average property of each phase can by analytically obtained, for a multi-phase material, by fitting the experimental frequency distribution of the mechanical property either with the theoretical probability density function (PDF) or the cumulative distribution function (CDF). Only those phases whose peak intensity is much higher than the background noise will be detected in a statistically consistent way.

Starting from the original idea, the method has been further implemented and optimised in the last ten years by several research groups [29–41]. LD and HD C-S-H phases in cement pastes have been recently identified by the use of this method and the analysis of the elastic modulus maps [42–44]. Previous papers also showed that fitting of the cumulative distribution functions (CDF) (Fig. 1b) is statistically more reliable, in comparison with the PDF, because CDF analysis does not require the choice of a bin-size to build the frequency histogram.

Unfortunately, the reliability of statistical nanoindentation methods for mapping the mechanical properties of cement at the nanoscale is still debated, because the number of valid nanoindentation measurements obtainable in a reasonable time (usually <100 valid tests per day can be achieved) is insufficient to reduce the signal-to-noise ratio and to provide a quantitative and reliable analysis of the phases present in low amount (e.g. the UHD-C-S-H and the un-hydrated phases), whose peak intensity is usually of the same order of the noise associated to experiments.

In the present work, the hydration mechanisms of a commercial cement paste and the related nano-mechanical properties have been investigated by the use of an innovative statistical high-speed nanoindentation method. The two-dimensional analyses of mechanical phases, coupled with SEM-EDS maps have been statistically obtained with a high consistency by using a new nanoindentantion technique [45], which allows getting a significant number of valid tests in a very small time (roughly one entire load-unload nanoindentation cycle per second, meaning more than 50,000 tests in 24 h). The obtained data revealed a complex interaction between the single constituents and their mechanical properties. In addition, the behaviour of the elastic modulus of the single phases as a function of the hydration time has been investigated: the evolution of the cement paste mechanical resistance properties is found to be due to a variation of the volume proportions between the three principal binding phases (LD, HD and UHD C–S–H) and could be related to a gradual increase of the hydration internal products (HD and UHD C-S-H) with respect to the external products (LD C-S-H), being this increase the major responsible of the material resistance improvement.

2. Materials and methods

2.1. Sample preparation

Cement paste samples were produced from an ordinary Portland cement powder (OPC, CEM I 52.5R according to European standard EN 197-1), using a w/c ratio of 0.36 (deionized water was used). More details on the adopted cement can be found elsewhere [46–47].

The paste was cast into a cylindrical mould stored in a controlled humidity and temperature environment (RH > 95% and 20 °C) until several predetermined curing times (1–3–7–14 and 28 days) were achieved. Cylindrical samples of 9 mm thickness and 18 mm diameter were obtained using a high precision cutting machine.

2.2. Polishing procedures

All the samples were polished down to a surface roughness Ra, which resulted 10 ± 5 nm. As a consequence of this, an indentation depth of 100 nm (or higher) should not be significantly affected by roughness effects (Fig. 2). In order to get a quick, repeatable and high level of polishing without losing the right hydration level, a double-step polishing process was established: samples were first polished using a manual polisher without water (to avoid additional hydration) using successive diamond films of 30, 12 and 5 μm at 600 rpm (30 s each step). In the second step, samples were finely polished using a semi-automatic Minimet 1000 polishing machine and a Duratex film-cloth combined with a polycrystalline diamond suspension of 1 μm (0,5 ml of solution for 1–4 cycles of 90 s using a 1 lb load at 50 rpm).The combination of the two polishing steps was fundamental to achieve repeatable results with minimum artifacts. Surface morphology and surface roughness were measured by optical microscopy and confocal profilometer analyses. A Leica DCM 3D optical profilometer was used to calculate the surface roughness parameters of interest.

2.3. Mechanical characterization

Nanoindentation tests were performed using a Keysight G200 Nano Indenter, equipped with a Nano-positioning stage, DCM II head with a Berkovich tip, equipped with both CSM (Continuous Stiffness Measurement) and high-speed (express test) options. Nanoindenter frame stiffness and tip area function were calibrated by testing on a fused quartz reference sample, according to the ISO 14577 standard.

In case of standard CSM tests, a grid of 20×20 indents was realized over a squared area of 200×200 μm^2, with a spacing of 10 μm and a maximum indentation depth of 100 nm. CSM testing required about 72 h of nanoindenter working time, each indentation lasting about 10 min. CSM tests were useful to identify the optimal indentation depth, which reduces both the effects of surface roughness (more evident at shallower depths) and the ones due to porosity (more important at larger depths) on the modulus vs depth profile: 100 nm was found to

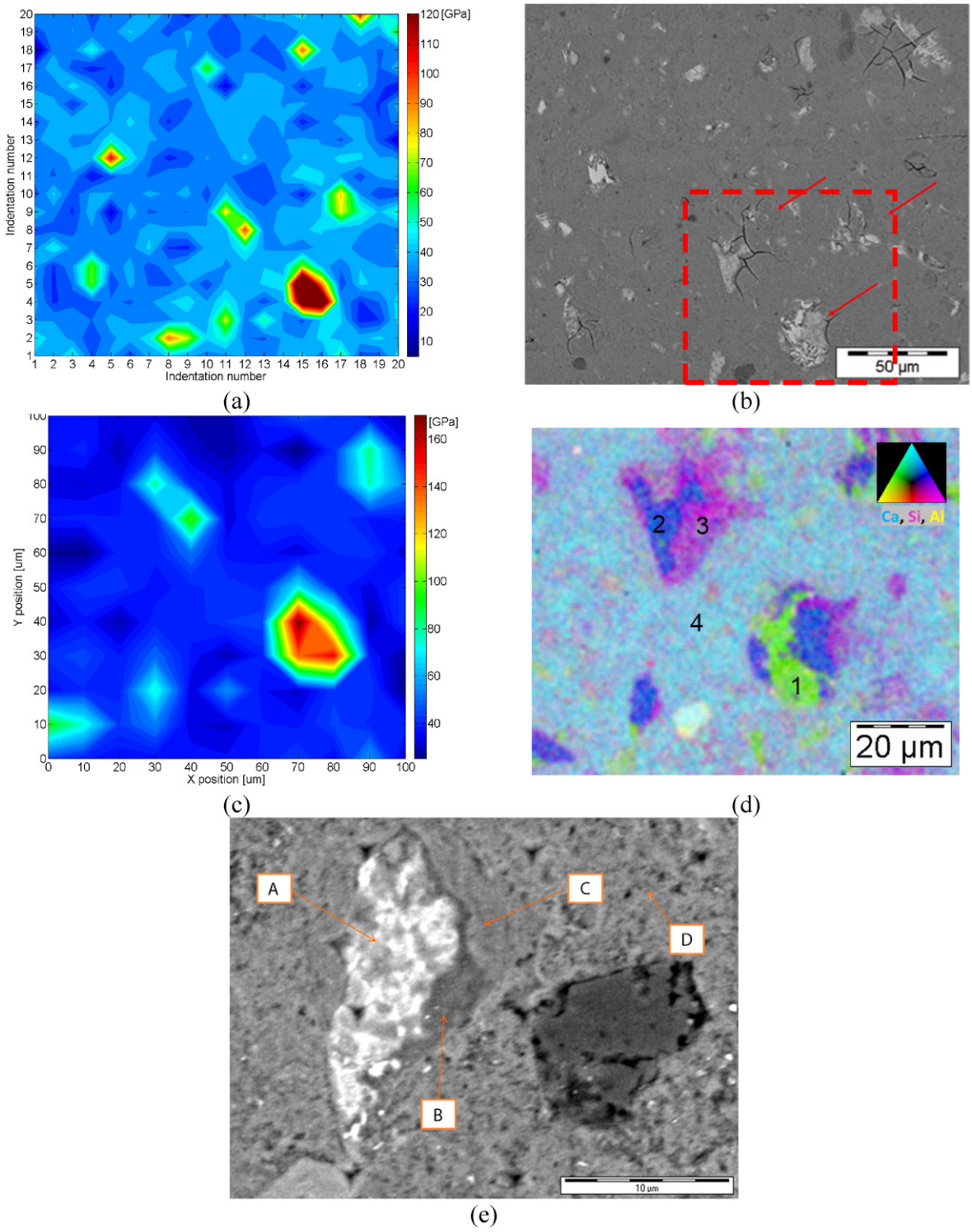

Fig. 4. (a) Elastic modulus map (GPa), as obtained by the conventional CSM (10 × 10 = 100 indents matrix, spacing 10 μm, indentation depth 100 nm). (b) SEM micrograph of the corresponding zone of the Elastic modulus map. (c) Elastic modulus map of the red squared zone. (d) SEM-EDS map of the same area, where the green phase corresponds to C_4AF clinker phases (label 1), the blue one to C_3S clinker phase (label 2), the violet and light-blue to the HD and LD C-S-H, labels 3 and 4. (e) SEM micrograph with all the four main phases in evidence: A (un-hydrated clinker), B (UHD C–S–H), C (HD C–S–H), D (LD C–S–H). The maps in these figures correspond to 28 days of hydration.

be the optimal depth, giving the most reliable evaluation of elastic modulus for such materials.

High-speed tests were obtained by setting up multiple arrays of 50 × 50 indents, over an area of 100 × 100 μm^2, with a maximum depth of 100 nm and a spacing of 2 μm. After a series of testing on fused silica reference samples, the selected spacing was verified to be sufficient to avoid any mutual influence between indents, at least for the ceramic materials under investigation (which show a low E/H value and therefore a low constraint factor [48]).

High-speed nanoindentation performs one complete indentation cycle per second, including approach, contact detection, load, unload, and movement to the next indentation site.

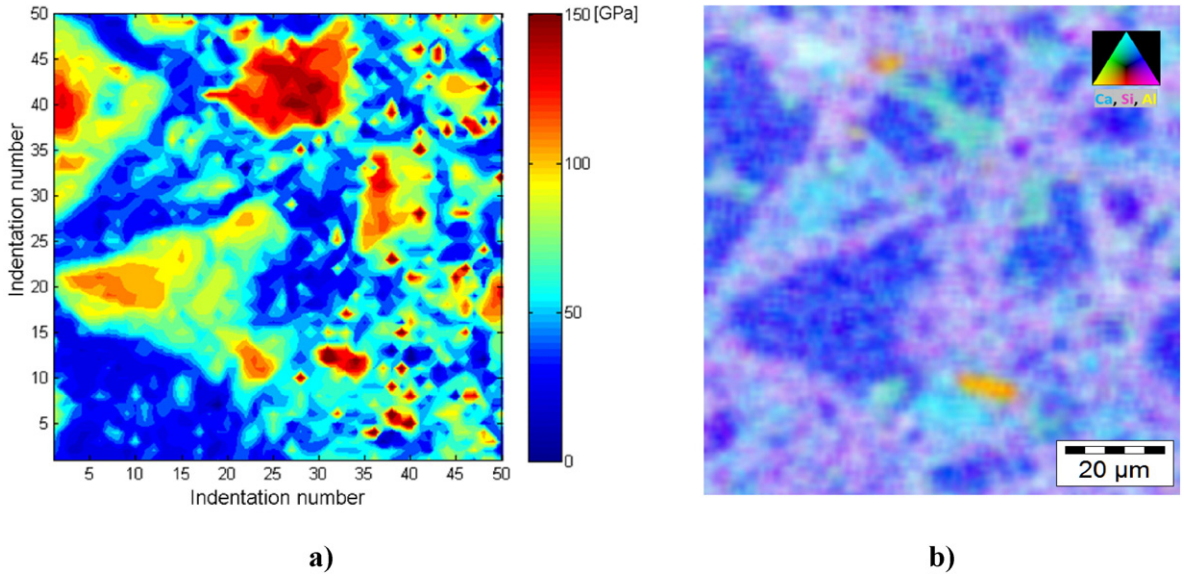

Fig. 5. (a) Elastic modulus map (GPa), as obtained by the High-speed method (50 × 50 = 2500 indents matrix, spacing 2 μm, indentation depth 100 nm), (b) SEM-EDS map of the same area, where the purple phase corresponds to C4AF clinker phases, the yellow to C3S clinker phase. This map corresponds to 1 day of hydration.

In this work, fifteen different matrices were performed in a single day of testing (ten hours), being the overall number of performed tests equal to 37,500. Examples of high-speed and conventional maps are presented in Fig. 3.

Statistical deconvolution on the Cumulative Distribution Functions (CDF) is then performed to obtain the number, distribution and elastic moduli of the mechanical phases in the material. The same procedure reported in the literature [28] was used for both the standard and the high-speed nanoindentation data.

2.4. Morphological and chemical characterization

Detailed microstructural and compositional observation of the same areas of the nanoindentation maps were finally obtained by SEM-EDS analysis, with the final purpose to study the correlation between composition and the mechanical properties of the hydration products of cement. A FEI SEM XL30 equipped with EDS was used to obtain images of the surface morphology and the chemical composition of the samples. EDS analysis were made at 20 kV of accelerating voltage, DT 20%, CPS 10,000, time constant 20. The obtained 2D EDS maps are fundamental to couple the results obtained with Nanoindentation analysis.

3. Results

Results from roughness analysis on the polished samples are reported in Fig. 2. A roughness (Ra) in the range of 5–15 nm was measured for all samples. This is a confirmation that nanoindentation data acquired at 100 nm of indentation depth can be considered as reliable [48].

The results obtained by means of Conventional Test and High-Speed nanoindentation are reported in Figs. 4 and 5, respectively. In both cases, a good correspondence between the elastic modulus maps and the SEM-EDS observations is observed. The full information on chemical element percentage on this kind of cement paste is reported in previous papers [46–47]. A comparison between the two methods is also reported in Tables 1–2. An optical observation of all performed maps for a given sample (both conventional and high-speed) is reported in Fig. 3.

Although the positions of the un-hydrated grains are clearly identified, it was not possible to identify them in the deconvolution of Conventional CSM map (Fig. 4a), as reported in Fig. 7, because of the insufficient number of experiments in this case. In addition, no distinction is possible among the tri- and di-calcium silicates (C_2S and C_3S), the calcium aluminate and ferrite (C_3A and/or C_4AF) in conventional indentation tests.

Conversely, a very detailed 2D map of elastic modulus distribution is obtained by high-speed nanoindentation in all cases, as reported in Fig. 5. In this case, statistical deconvolution of experimental data gave detailed information on four different mechanical phases, as reported in Fig. 8, that were identified as (a) un-hydrated clinker, (b) UHD C–S–H, (c) HD C–S–H and (d) LD C–S–H.

The SEM-EDS maps reported in the Fig. 4d show the presence of a C_3S grain (label 2 upper left), a mixed C_3S/C_4AF grain (label 1 bottom right), a magnesium oxide (MgO) particle (white particle) and three smaller C_3S grains. The inner product of hydration (High-Density-C-S-H and Ultra-High-Density-C-S-H) is clearly recognizable as the violet (Si-rich) crown around the un-hydrated C_3S grains. The low-density-C-S-H (Ca-rich) is the light blue matrix. The elemental distribution in the EDS maps was not observed previously.

In addition, the use of high-speed nanoindentation allowed investigating the nanomechanical properties of the same cement paste at the early stages of hydration.

As reported in the Fig. 9, no significant variation with time of the absolute values of the elastic moduli is observed, as a confirmation of the

Table 1
Average elastic moduli of the hydrated phases (standard CSM method).

Phase	E (standard CSM test) [GPa]
HD C–S–H	39.3 ± 2.8
LD C–S–H	30.1 ± 2.3

Table 2
Average elastic moduli of the hydrated phases (express test method).

Phase	E (High-speed test) [GPa]
Clinker	104.0 ± 9.7
UHD C–S–H	76.2 ± 9.1
HD C–S–H	47.6 ± 6.2
LD C–S–H	30.8 ± 3.5

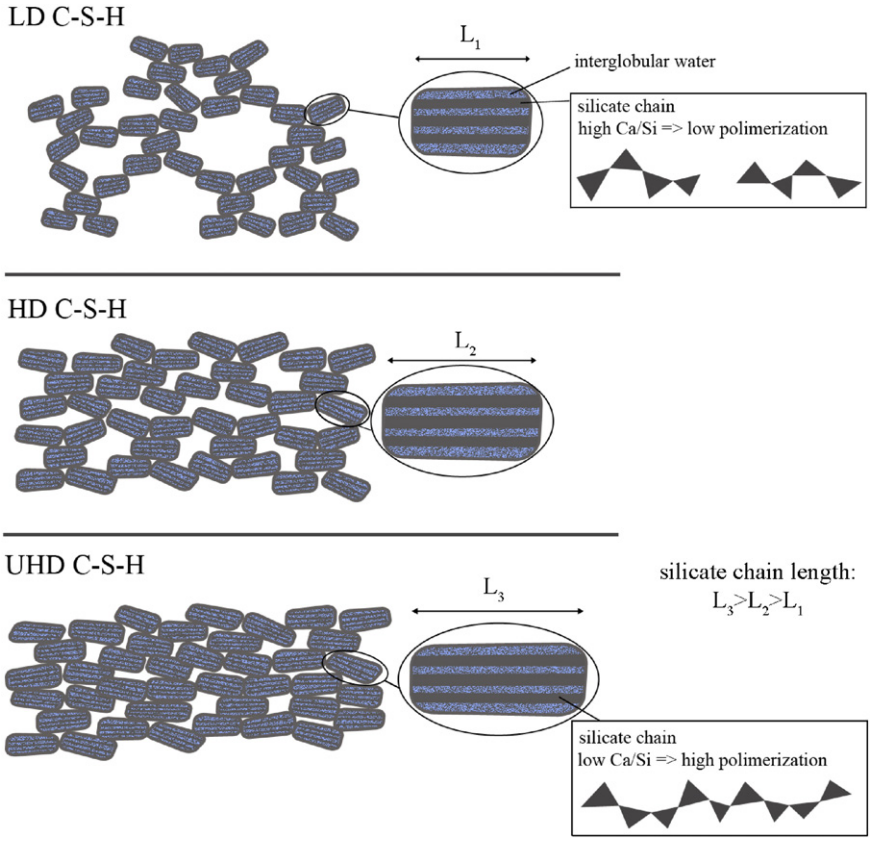

Fig. 6. Schematic representation of the microstructure of LD C–S–H, HD C–S–H and UHD C–S–H.

assumption that the number of hydrated phases in cement pastes correspond to discrete levels of packing densities, as described in the following chapter.

4. Discussion

In this work, a novel high-speed nanoindentation mapping technique is used to investigate the hydration mechanisms of a cement paste, as a function of time and in comparison with EDS maps.

In contrast with the conventional low-resolution maps, reported in Fig. 4, an excellent correspondence is noticed between the mechanical map (Fig. 5a) and the SEM-EDS map (Fig. 5b) in case of high-speed nanoindentation. In this latter case, a clear distinction between C_3S and mixed C_3S/C_4AF grains was possible, as reported in Fig. 5a and confirmed by EDS analysis (Fig. 5b). All these particles are clearly defined by the high-speed mapping, where the elastic modulus gradients inside single phases are also well defined. In particular, higher modulus is found for the C_4AF with respect to the C_3S un-hydrated grains. Clear distinctions in terms of elastic modulus at the boundaries of un-hydrated particles are also observed, which probably correspond to the high-density C-S-H phases. Since only a few particles are tested within the maps, we cannot exclude the presence of the other un-hydrated clinker grains (C_2S and C_3A).

EDS maps (Fig. 4d) also show that the concentration of Si in High Density C–S–H phases is higher than that in LD C–S–H (lower Ca/Si ratio), with a more homogeneous spatial distribution. This finding is in agreement with some recent papers demonstrating, both theoretically and experimentally, that the calcium silicate hydrate phase showing

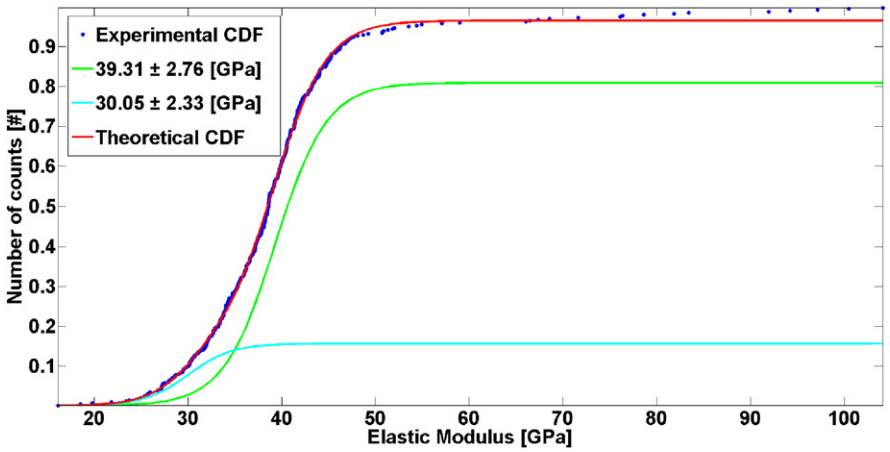

Fig. 7. Cumulative distribution function (CDF) analysis on 399 valid indents obtained by the conventional CSM method at 100 nm depth.

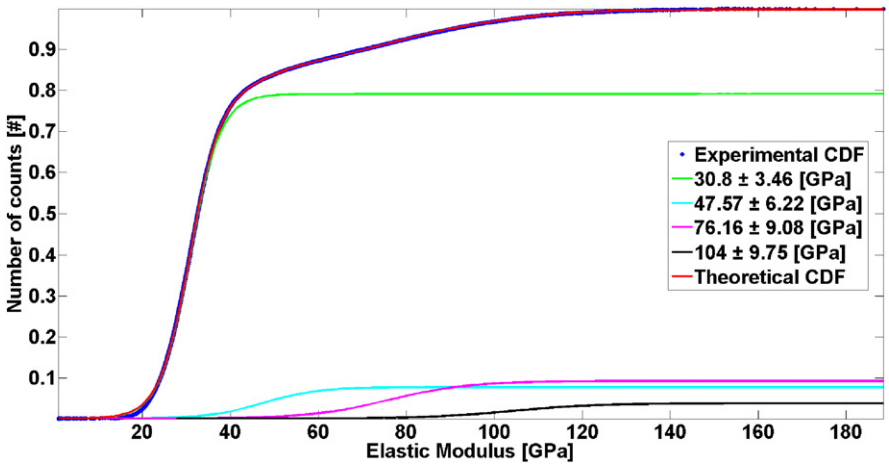

Fig. 8. Cumulative distribution function (CDF) analysis on 37,500 valid indents obtained by the express method at 100 nm depth.

the highest hardness and elastic modulus (High Density C–S–H phases) have the lowest Ca/Si ratio. In particular, Manzano [49] et al. reported an atomistic description of C–S–H, based on force field models and showed that the elastic modulus of this phase increases with increasing the length of the silicate chain, i.e. as Ca/Si decreases. Furthermore, Pelisser et al. synthesized C–S–H phases with different Ca/Si and studied their micro/nanomechanical characteristics [50]. In their work, they verified that the elastic modulus and hardness increase with the decreasing of the Ca/Si molar ratio. The results provided in this work further confirm that also in real Portland cement samples the HD (and UHD) C–S–H (i.e. the phases with the best mechanical properties) shows a Ca/Si ratio lower than LD C–S–H, which means that the silicate chains constituting the basic globules of the high density phases are, on average, longer than those in the low density one. According to these results, as represented in Fig. 6, the improved mechanical properties of high density C–S–H with respect to those of LD C–S–H stem from the combination of two main reasons: i) a reduced porosity and ii) the increased length of the elemental globules, due to the lower Ca/Si ratio.

The use of the high-speed nanoindentation approach is a real enabling technology for this application, as it allows achieving real micron-scale spatial resolution for mechanical property mapping. This is further confirmed by the statistical deconvolution analysis reported in the Figs. 7 and 8. The output data from the nanoindenter were used to calculate the statistical deconvolution of the Elastic Modulus values.

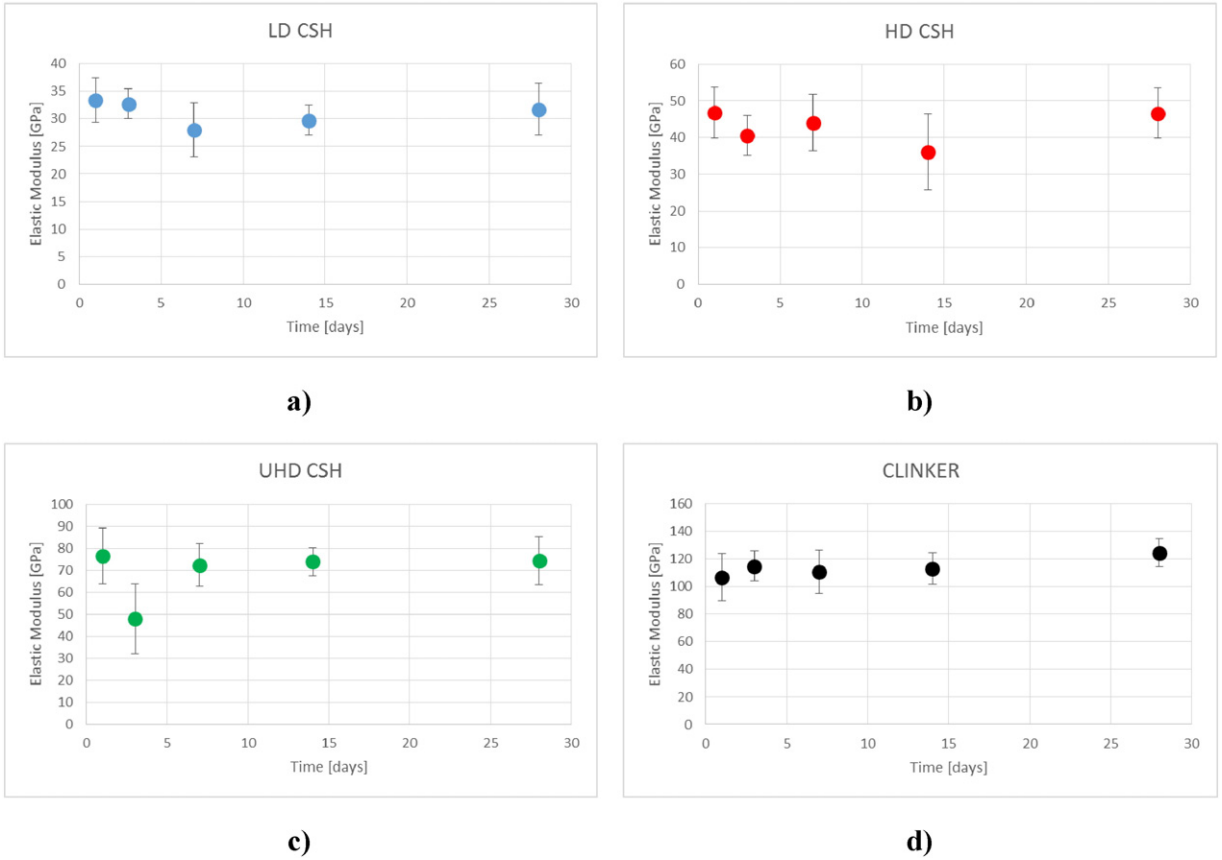

Fig. 9. Average elastic moduli values in the different hydration times for the different phases: LD C-S-H (a), HD C-S-H (b), UHD C-S-H (c) and clinker (d).

Table 3
Average elastic moduli of the hydrated phases at different hydration days.

Hydration time [days]	E [GPa] LD C–S–H	E [GPa] HD C–S–H	E [GPa] UHD C–S–H	E [GPa] clinker
1	33.4 ± 4.1	46.9 ± 6.9	76.4 ± 12.6	106.9 ± 17.2
3	32.7 ± 2.7	40.5 ± 5.4	47.9 ± 15.8	114.9 ± 10.8
7	28.0 ± 4.9	44.0 ± 7.6	72.3 ± 9.7	111.0 ± 15.7
14	29.7 ± 2.7	36.1 ± 10.3	73.8 ± 6.4	113.3 ± 11.6
28	31.6 ± 4.6	46.6 ± 6.8	74.4 ± 10.8	124.6 ± 10.3

By means of the standard CSM method, only 2 phases could be reliably obtained from the statistical analysis, while with the High-Speed method 4 phases were recognized. This is due to the difficulty to get stable statistical results with only 400 indentations obtained with the standard method, not enough to distinguish the various C–S–H phases or the unhydrated clinker (the peaks associated to these phases could be often of the same order of the noise of the tests). The stability of the results is calculated by several fittings between the experimental results and the theoretical cumulative distributions.

The example reported in the Fig. 8 is the one with the lowest fitting error. Note that previous literature studies report similar data [28], with elastic modulus values for the four phases (LD-C-S-H, HD-C-S-H, UHD-C-S-H and un-hydrated clinker) being equal to 22.5, 30.4, 40.9 and 93.4 GPa, respectively.

The value of elastic modulus attributed to UHD-C-S-H in the present experiments is especially higher than the previously reported estimation, a difference that cannot simply explained by considering the higher strain rate that is applied during high-speed indentation, that may even induce a sort of thermally activated deformation mechanism. The value obtained here (~76 GPa) approaches those of the crystalline phases that more realistically describe the short-range order in C–S–H. A recent paper [51] systematically reports the molecular dynamics simulation of the elastic properties of the most important crystalline phases present in hydrated cement pastes. In particular the class of tobermorites and jennite minerals are reported to have Young modulus in the range 70–110 GPa. Also, applying the microporomechanical Mori-Tanaka equations, in order to account for the porosity of UHD-C-S-H, an estimated E value in the range 63–80 GPa is obtained using the tobermorite 9 Å and the tobermorite 11 Å structures, which are those with the lowest Ca/Si ratio. The presence of three different packing levels for the hydrated paste is also confirmed by the SEM micrograph reported in Fig. 4(e). On the other hand, the analysis of 37,500 valid tests obtained by the high-speed method (Fig. 8) gives extremely robust results, irrespective of the adopted deconvolution approach (PDF and CDF): in both cases, the peaks corresponding to four main phases are identified in a reproducible way, being the intensity of all the peaks significantly higher than the noise associated to measurements.

Therefore, the most reliable mechanical properties of the cement paste are those given in the Fig. 8: four main phases are identified, namely the LD-C-S-H, HD-C-S-H, UHD-C-S-H and un-hydrated clinker. This attribution is in agreement with results in the literature [28].

Finally, it is interesting to make a quantitative comparison between the average elastic moduli of the hydrated phases, as obtained by the conventional and high-speed methods.

Results of the average elastic moduli of the four phases for each hydration time chosen (1, 3, 7, 14, 28 days) are reported in Fig. 9 a-d and Table 3. It is evident that the values are not consistently changing during the time: this agrees with previous studies [28,52] that confirm the presence of different (and discrete) packing densities for the C–S–H phases obtained during the hydration process. These packing levels have their own limit densities ruled by the structural arrangement that the elementary particle of C–S–H could assume: compact random packing, with maximum density $\eta \approx 0.64$, for the LD C–S–H; face-centered cubic (CFC) or hexagonal close-packed (HCP), with maximum density $\eta \approx 0.74$, for the HD C–S–H; packing density of $\eta = 0.83$ for UHD C–S–H phase [28]. Assuming the constancy of the single phases, considering the hydration mechanism, what changes with time is the proportion between them. In particular the increasing of the hydration internal products (HD C–S–H and UHD C–S–H) compared to the external products (LD C–S–H) could be assumed to be responsible for the usually observed trend of macroscopic properties with hydration time.

5. Conclusion

In this work, the hydration mechanisms of a commercial cement paste have been investigated by means of an innovative statistical high-speed nanoindentation method.

The new method significantly improves statistical reliability and spatial resolution when mapping the mechanical properties of the samples by nanoindentation, given the very high number of valid experiments that can be made in a single day of testing (more than 35,000).

The two-dimensional nanomechanical mapping on Portland cement paste samples, coupled with SEM-EDS maps, revealed the presence of three distinct hydrated phases (low density, high-density and ultra-high density C–S–H). High-density and ultra-high density phases correspond to the inner products of hydration, while the low-density phase is the outer hydration product. By correlation with SEM-EDS observations, the different packing densities were also correlated to different Ca/Si ratios.

In addition, results showed that the intrinsic elastic moduli of the hydrated C-S-H phases are independent on hydration time, thus confirming that they are uniquely related to discrete packing density levels.

The results presented here demonstrate that high-speed nanoindentation mapping is a reliable experimental tool that can be an enabling technology for the design of innovative cement formulations, e.g. by tailoring the relative content of the constituents and/or addition of nano-additives.

References

[1] H. Taylor, Cement Chemistry, Thomas Telford Publishing, London, 1997.
[2] A.J. Allen, J.J. Thomas, H.M. Jennings, Nat. Mater. 6 (2007) 311–316.
[3] W.-S. Chiang, G. Ferraro, E. Fratini, F. Ridi, Y.-Q. Yeh, U.S. Jeng, S.-H. Chen, P. Baglioni, Multiscale structure of calcium-and magnesium-silicate-hydrate gels, J. Mater. Chem. A 2 (32) (2014) 12991–12998.
[4] H.M. Jennings, Cem. Concr. Res. 38 (2008) 275–289.
[5] S. Xiang, et al., Hybrid effects of carbon fibers on mechanical properties of Portland cement mortar, Mater. Des. 65 (2015) 1222–1228.
[6] Soto-Pérez Linoshka, V. López, Sangchul S. Hwang, Response surface methodology to optimize the cement paste mix design: Time-dependent contribution of fly ash and nano-iron oxide as admixtures, Mater. Des. 86 (2015) 22–29.
[7] B. Lothenbach, K. Scrivener, R.D. Hooton, Cem. Concr. Res. 41 (2011) 1244–1256.
[8] J. Lee, S. Mahendra, P.J.J. Alvarez, ACS Nano 4 (2010) 3580–3590.
[9] W.C. Chiang, E. Fratini, F. Ridi, S.H. Lim, Y.Q. Yeh, P. Baglioni, S.M. Choi, U.S. Jeng, S.H. Chen, J. Colloid Interface Sci. 398 (2013) 67–73.
[10] P.-J. Han, S. Wang, F.Y. Chen, X. Bai, J. Cent. South Univ. 22 (5) (May 26 2015) 1869–1877, 2706.
[11] Thanongsak Nochaiya, Yoshika Sekine, Supab Choopun, Arnon Chaipanich, J. Alloys Compd. 630 (2015) 1–10.
[12] Ha Thanh Le, Matthias Müller, Karsten Siewert, Horst-Michael Ludwig, Mater. Des. 72 (2015) 51–62.
[13] G. Constantinides, F.-J. Ulm, Cem. Concr. Res. 34 (2004) 67–80.
[14] S. Haoyang, X. Jinyu, R. Weibo, Experimental study on the dynamic compressive mechanical properties of concrete at elevated temperature, Mater. Des. 56 (2014) 579–588.
[15] J.C. Shu, H.D. Wen, J. Zong, Tong Li, Bo Sui, New approach for characterisation of mechanical properties of cement paste at micrometre scale, Mater. Des. 87 (2015) 992–995.
[16] Jun Jiang, Zhongyuan Lu, Yunhui Niu, Jun Li, Yuping Zhang, Study on the preparation and properties of high-porosity foamed concretes based on ordinary Portland cement, Mater. Des. 92 (2016) 949–959.
[17] K. Velez, S. Maximilien, D. Damidot, G. Fantozzi, F. Sorrentino, Cem. Concr. Res. 31 (2001) 555–561.
[18] H.M. Jennings, J.J. Thomas, J.S. Gevrenov, G. Constantinides, F.J. Ulm, Cem. Concr. Res. 37 (2007) 329–336.
[19] H.M. Jaeger, S.R. Nagel, Physics of the granular state, Science 255 (5051) (1992) 1523–1531.
[20] N.J.A. Sloane, Kepler's conjecture confirmed, Nature 395 (1998) 435–436.
[21] R.J.-M. Pellenq, H. Van Damme, MRS Bull. 29 (2004) 319–323.
[22] I.G. Richardson, Cem. Concr. Res. 38 (2008) 137–158.

[23] E. Cappelletto, S. Borsacchi, M. Geppi, F. Ridi, E. Fratini, P. Baglioni, J. Phys. Chem. C 117 (2013) 22947–22953.
[24] D. Bonen, S. Diamond, J. Am. Ceram. Soc. 77 (1994) 1875–1882.
[25] J.J. Hughes, P. Trtik, Mater. Charact. 53 (2004) 223–231.
[26] I.G. Richardson, G.W. Groves, J. Mater. Sci. 28 (1993) 265–277.
[27] P. Acker, Creep, Shrinkage and Durability Mechanics of Concrete and Other Quasi-Brittle Materials: Proceedings of the Sixth International Conference, Concreep-6 Mit, Elsevier Science Limited, Cambridge (Ma), USA, August 20–22, 2001 2001.
[28] M. Vandamme, F.-J. Ulm, P. Fonollosa, Cem. Concr. Res. 40 (2010) 14–26.
[29] L. Sorelli, G. Constantinides, F.-J. Ulm, F. Toutlemonde, Cem. Concr. Res. 38 (2008) 1447–1456.
[30] P. Mondal, S.P. Shah, L.D. Marks, ACI Mater. J. (2008) 105.
[31] C. Plassard, E. Lesniewska, I. Pochard, A. Nonat, Ultramicroscopy 100 (2004) 331–338.
[32] P. Mondal, S.P. Shah, L. Marks, Cem. Concr. Res. 37 (2007) 1440–1444.
[33] M. Vandamme, F.J. Ulm, Proc. Natl. Acad. Sci. 106 (2009) 10552–10557.
[34] M. Miller, C. Bobko, M. Vandamme, F.J. Ulm, Cem. Concr. Res. 38 (2008) 467–476.
[35] M.J. DeJong, F.-J. Ulm, Cem. Concr. Res. 37 (2007) 1–12.
[36] W. Zhu, J.J. Hughes, N. Bicanic, C.J. Pearce, Mater. Charact. 58 (2007) 1189–1198.
[37] P. Trtik, B. Münch, P. Lura, Cem. Concr. Compos. 31 (2009) 705–714.
[38] J.J. Chen, L. Sorelli, M. Vandamme, F.-J. Ulm, G. Chanvillard, J. Am. Ceram. Soc. 93 (2010) 1484–1493.
[39] N.X. Randall, M. Vandamme, F.-J. Ulm, J. Mater. Res. 24 (2011) 679–690.
[40] M. Vandamme, F.-J. Ulm, Cem. Concr. Res. 52 (2013) 38–52.
[41] W.R.L. da Silva, J. Němeček, P. Štemberk, Adv. Eng. Softw. 62–63 (2013) 109–118.
[42] G. Constantinides, Mater. Struct. 36 (2003) 191–196.
[43] F.-J. Ulm, Mater. Struct. 37 (2003) 43–58.
[44] F.-J. Ulm, M. Vandamme, C. Bobko, J. Alberto Ortega, K. Tai, C. Ortiz, J. Am. Ceram. Soc. 90 (2007) 2677–2692.
[45] M.Z. Mughal, R.A. Moscatelli, H.Y. Amanieu, Marco Sebastiani, Effect of lithiation on micro-scale fracture toughness of LixMn2O4 cathode, Scr. Mater. 116 (2016) 62–66.
[46] M. Berra, F. Carassiti, T. Mangialardi, A.E. Paolini, M. Sebastiani, Leaching behaviour of cement pastes containing nanosilica, Adv. Cem. Res. 25 (6) (2013) 352–361.
[47] M. Berra, F. Carassiti, T. Mangialardi, A.E. Paolini, M. Sebastiani, Effects of nanosilica addition on workability and compressive strength of Portland cement pastes, Constr. Build. Mater. 35 (2012) 666–675.
[48] A. Bolshakov, G.M. Pharr, Influences of pileup on the measurement of mechanical properties by load and depth sensing indentation techniques, J. Mater. Res. 13 (4) (Apr 1998).
[49] H. Manzano, J.S. Dolado, A. Ayuela, Acta Mater. 57 (2009) 1666–1674.
[50] F. Pelisser, P.J.P. Gleize, A. Mikowski, J. Phys. Chem. C 116 (2012) 17219–17227.
[51] S. Hajilar, B. Shafei, Nano-scale investigation of elastic properties of hydrated cement paste constituents using molecular dynamics simulations, Comput. Mater. Sci. 101 (2015) 216–226.
[52] G. Constantinides, F. Ulm, J. Mech. Phys. Solids 55 (1) (2007) 64–90.